Electronic Supplementary Material (ESI) for Physical Chemistry Chemical Physics.

Supplementary Materials

The structural diversity of C-rich DNA aggregates: unusual self-assembly of beetle-like nanostructures

Anna D. Protopopova, Vladimir Tsvetkov, Anna M. Varizhuk, Nikolay A. Barinov, Victor V. Podgorsky, Dmitry V. Klinov, and Galina E. Pozmogova

HPLC analysis of C_nT_{25} oligonucleotides

The retention times (RT) of C_nT_{25} monomers agreed well with the calibration data obtained using synthetic nonstructured (according to CD) oligonucleotides of average sequence, amplicons, and plasmid DNA, while the RT calculated for intermolecular structures turned out to be significantly overestimated. Accordingly, we had to embed a correction to the calibration curve based on theoretical preconditions and AFM experimental data (red line in Figure S1a). For instance, C_5T_{25} had a peak at RT=11.8 min which should be related to a tetramer M•4, but not a dimer M•2. In the profile of C_7T_{25} (Figure S1b) we could recognize two separate peaks, from which one peak was related to a tetramer while the other was interpreted as a trimer M•3.

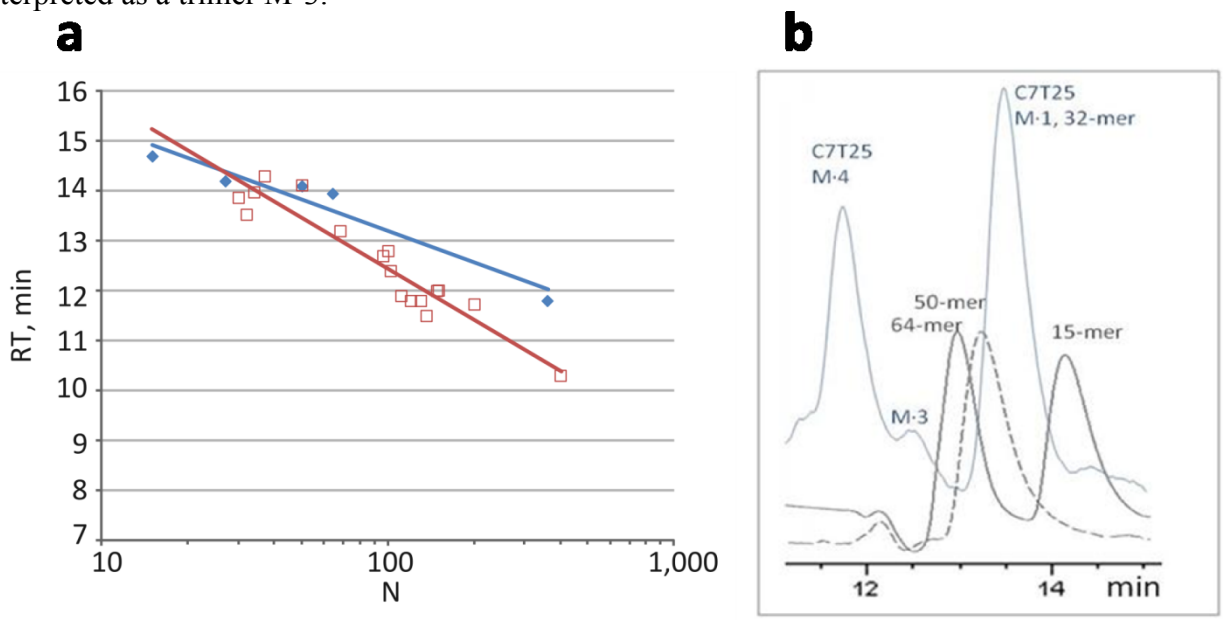

Figure S1. Correction of HPLC calibration curve. **a,** A fragment of the calibration curve of the GF-250 gel filtration column obtained with synthetic nonstructured (by CD spectra) oligonucleotides, ds DNA (150–200 bp), and plasmids (blue) and the corrected calibration curve (red). **b,** HPLC-profiles of control oligonucleotides and rapidly annealed C_7T_{25}.

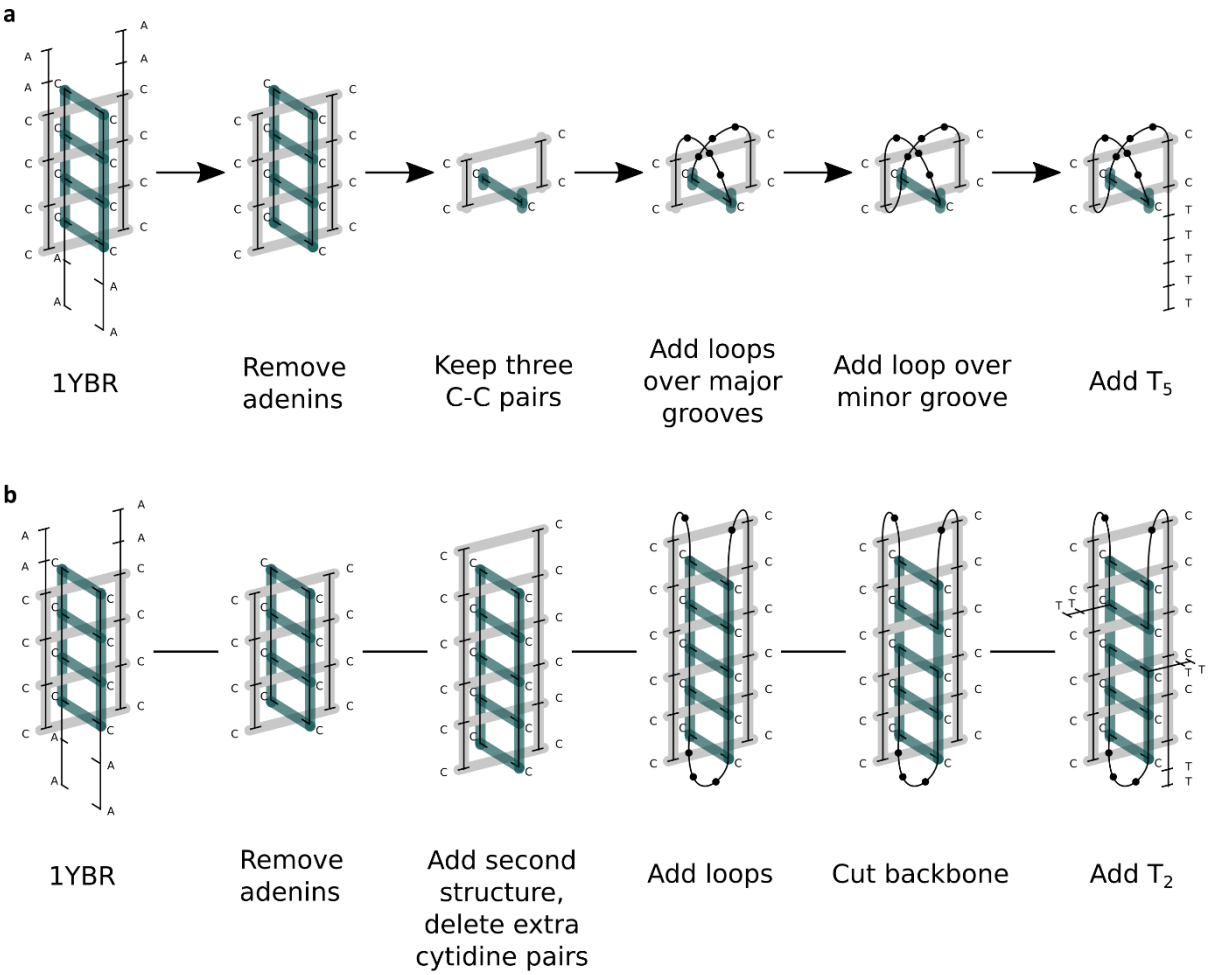

Figure S2. Schematics showing preparation of strating models for MD symilation. a, $C_{12}T_5$ monomer. **b,** C_9T_2 trimer.

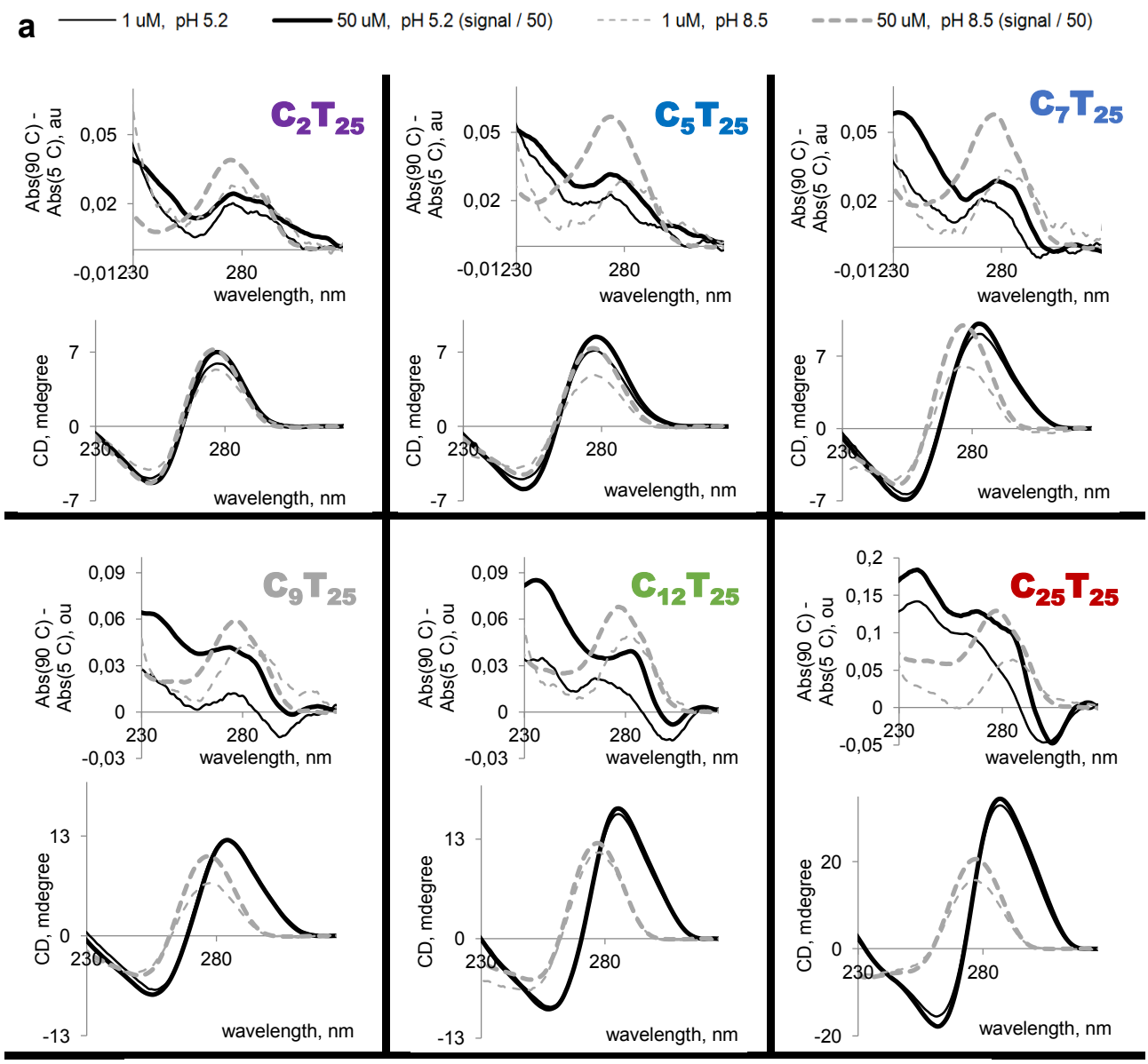
a
1 uM, pH 5.2
50 uM, pH 5.2 (signal / 50)
1 uM, pH 8.5
50 uM, pH 8.5 (signal / 50)
C2T25
C5T25
C7T25
C9T25
C12T25
C25T25
Abs(90 C) - Abs(5 C), au
Abs(90 C) - Abs(5 C), ou
CD, mdegree
wavelength, nm
b
1uM_melting
1uM_annealing
4uM_melting
4uM_annealing
25uM_melting
25uM_annealing
50uM_melting
50uM_annealing
ΔCD at 285 nm, %
temperature, °C

Figure S3. Concentration dependency of i-motif formation. a, TDS and CD spectra (5°C) of the oligonucleotide samples subjected to slow annealing. Conditions: 10 mM NaOAc (pH

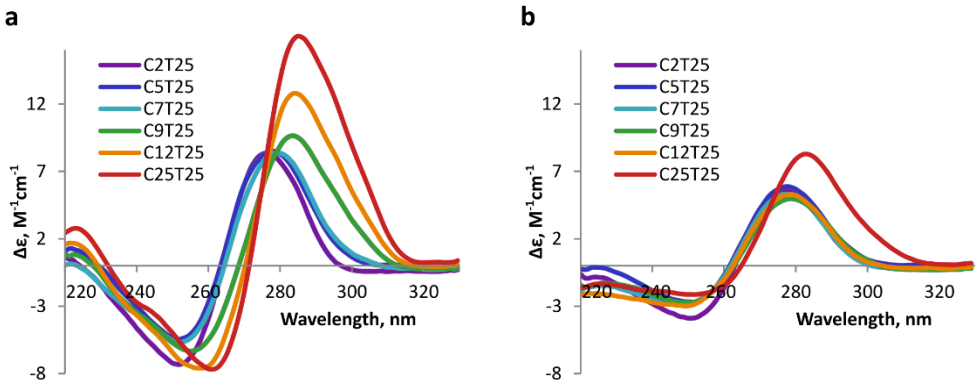

5.2) or 10 mM Tris-HCl (pH 8.5), 10 mM KCl. **b,** Annealing and melting curves. Conditions: 10 mM NaOAc (pH 5.2), 10 mM KCl. ON concentrations are specified in the legends.

Figure S4. CD spectra of rapidly annealed samples: a, obtained at 5°C. **b,** at 90°C. Ellipticity is given per mole of nucleotide.

AFM analysis of multimer's height

I-motif cores of all multimers formed from C_nT_{25} oligonucleotides were expected to have identical diameter. However, height of various i-motif multimers measured on our AFM images was essencially and reproducibly different. A prominent example is a histogram of $C_{25}T_{25}$ heights shown in Figure S5b. The peak at 0.5 nm corresponded to the single-stranded T_{25} appendages; i-motif monomers M•1 displayed a height greater than ssDNA, but still below 1 nm; a height of intermolecular i-motifs M•2, M•3, and M•4 varied considerably and entangled, but generally M•2 were lower than M•4 (about 1.2–1.3 nm versus 1.8–2.0 nm, respectively); the heights of M•5, M•6, and M•7 reached 2.5 nm. We hypothesize that high-order structures, such as M•4–M•7, are more stable than M•1–M•3 and therefore were less deformed during adsorption to the substrate surface. Additionally, T_{25} arms may contribute to the apparent i-motif height.

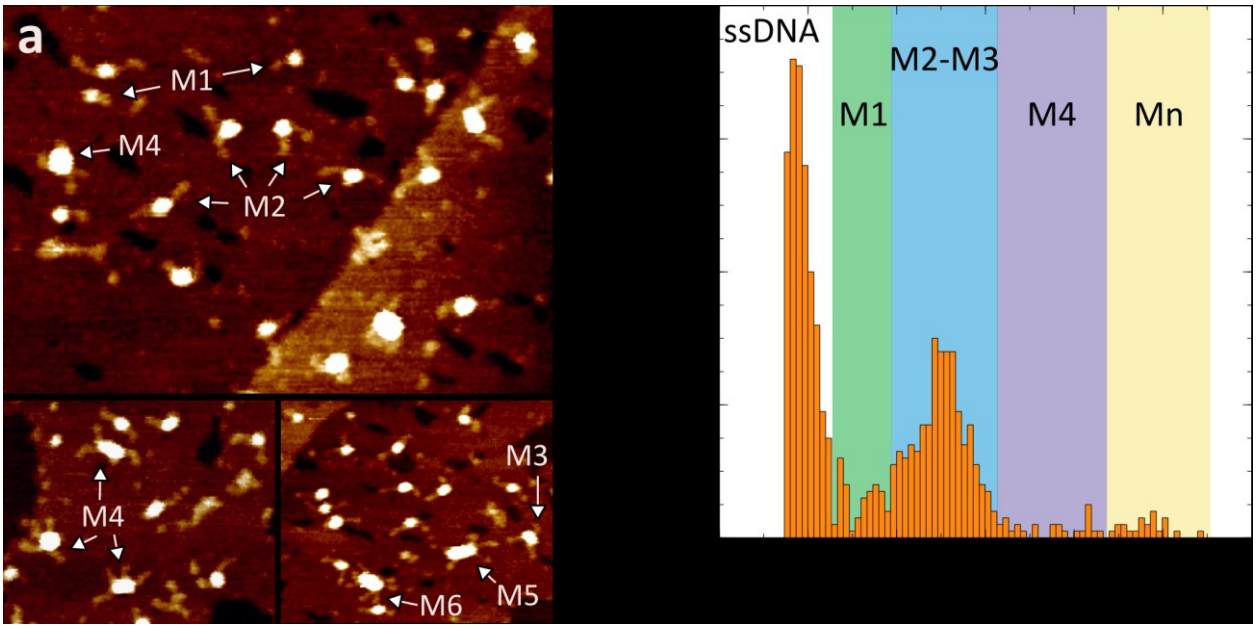

Figure S5. AFM analysis of I-motif height. a, AFM images of multimers formed from $C_{25}T_{25}$. **b,** heights distribution of i-motif cores and ssDNA appendages.

AFM analysis of i-motif stability at different pH

The pH dependence was analyzed with AFM. Increasing pH to 8.5 resulted in the unfolding of i-motifs in the samples of $C_{12}T_{25}$ and $C_{25}T_{25}$, but a small number of assembled monomers M•1 were found in both samples (Figure S6).

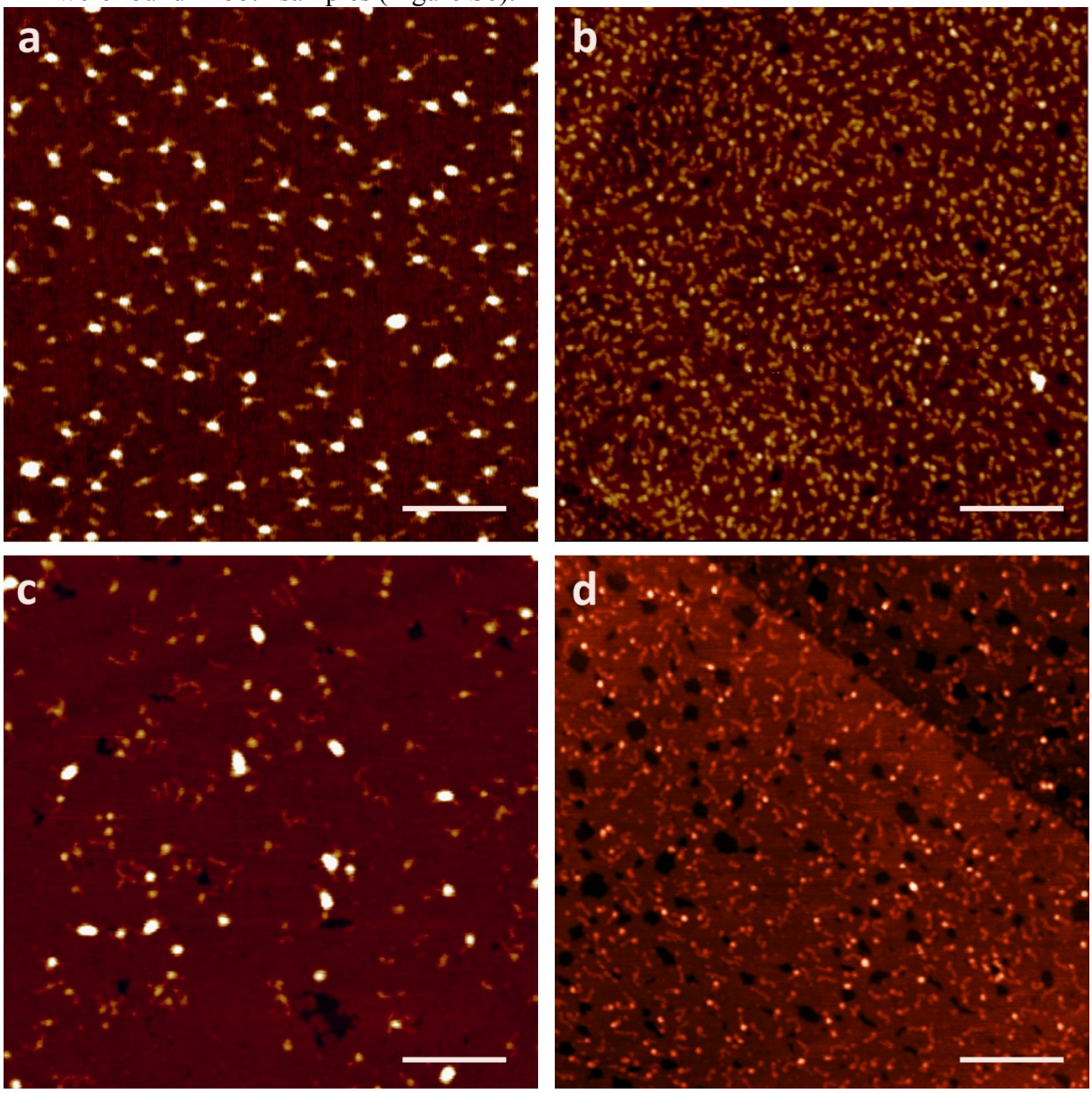

Figure S6. AFM evidence for pH-dependent disassembling of $C_{12}T_{25}$ and $C_{25}T_{25}$ nanostructures. a, $C_{12}T_{25}$, pH 5.5. **b,** $C_{12}T_{25}$, pH 8.5. **c,** $C_{25}T_{25}$, pH 5.5. **d,** $C_{25}T_{25}$, pH 8.5. The length of the scale bars is 100 nm.

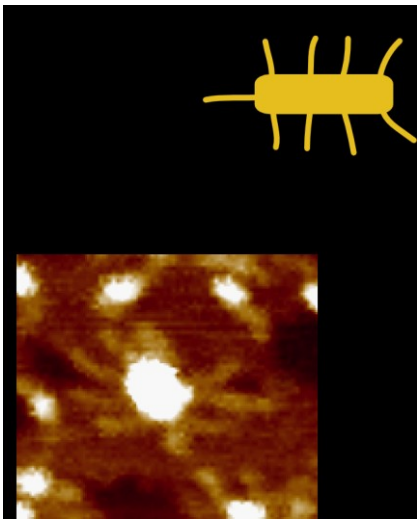

Figure S7. AFM image of $C_{25}T_{25}$ multimer comprised of nine oligonucleotides.

Figure S8. MD simulations of intermolecular i-motifs clarifying the structure of the loops: a-b, $C_{12}T_5$ monomer; **c-d,** $C_{10}T_5$ monomer; **e-f**, C_9T_2 dimer. Dynamics of a distance between the centers of mass of the bases forming each of the cytidine pairs and dynamics of the angle between the planes of the bases in the pairs.

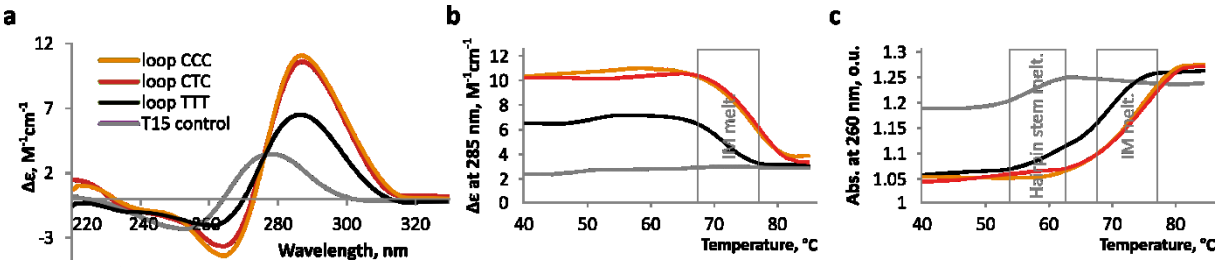

Figure S9. CD and UV data confirming formation of single-letter loops over the minor grooves of i-motifs. a, CD spectra obtained from rapidly annealed samples at 5°C. **b,** Thermal denaturation profiles by CD at 285 nm. **c,** Thermal denaturation profiles by UV adsorption at 260 nm.

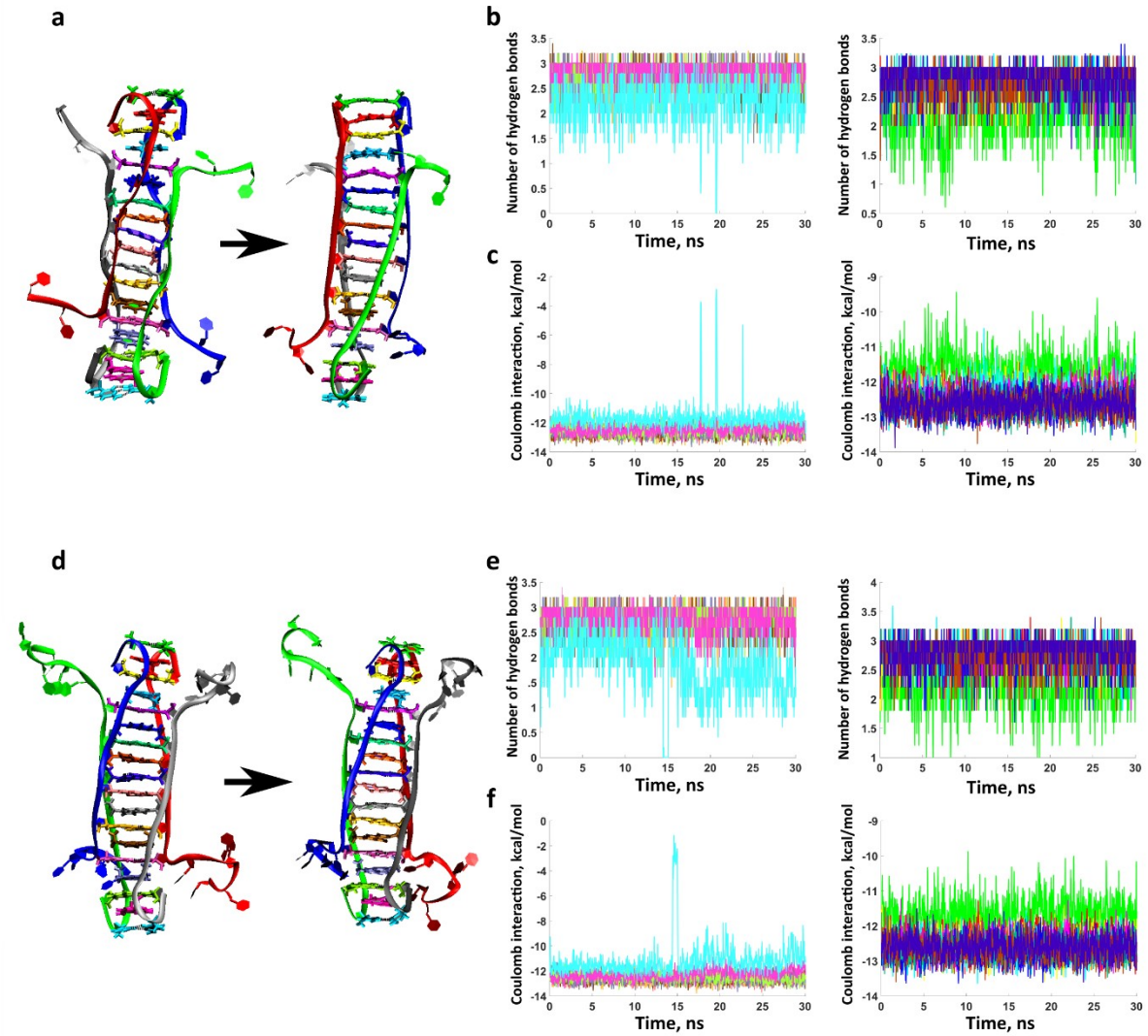

Figure S10. MD simulations of intermolecular i-motifs clarifying the stability of the hydrogen bonds between the loops: a-c, C_9T_2 tetramer; **d-f,** C_9T_5 tetramer. All simulations were performed for 30 ns and are presented with start and end conformations, dynamics of a number of hydrogen bonds between the bases forming each of the cytidine pairs, dynamics of the energy of electrostatic interaction between the bases in the pairs. In the schemes, cytidines connected with hydrogen bonds are colored in pairs, and colors correspond to the graphs of parameters. Due to the high number of pairs graphs of parameters are each split in two.

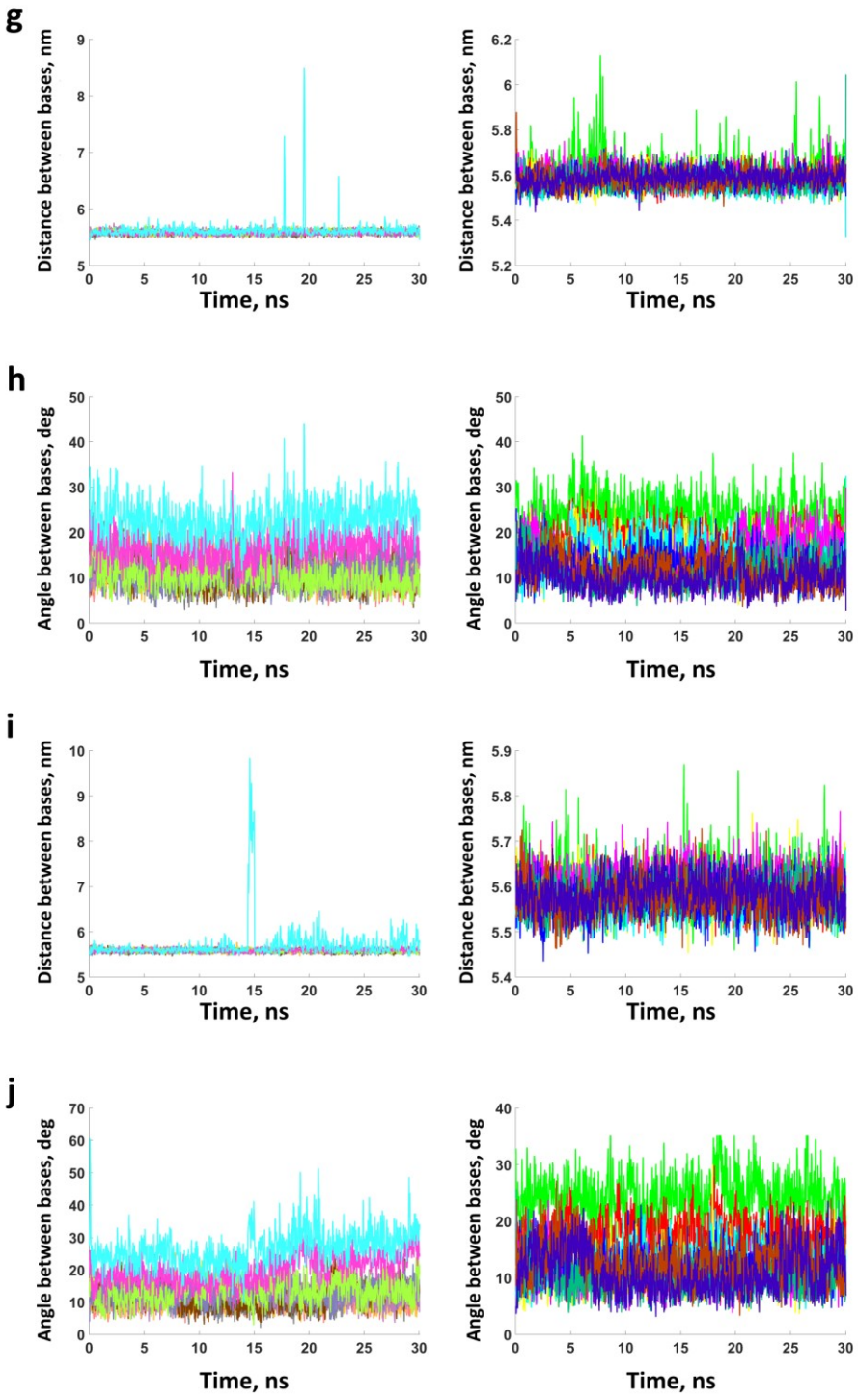

Figure S10. MD simulations of intermolecular i-motifs clarifying the stability of the hydrogen bonds between the loops (Continued): g-h, C_9T_2 tetramer; **i-j,** C_9T_5 tetramer. Dynamics of a distance between the centers of mass of the bases forming each of the cytidine pairs and dynamics of the angle between the planes of the bases in the pairs.

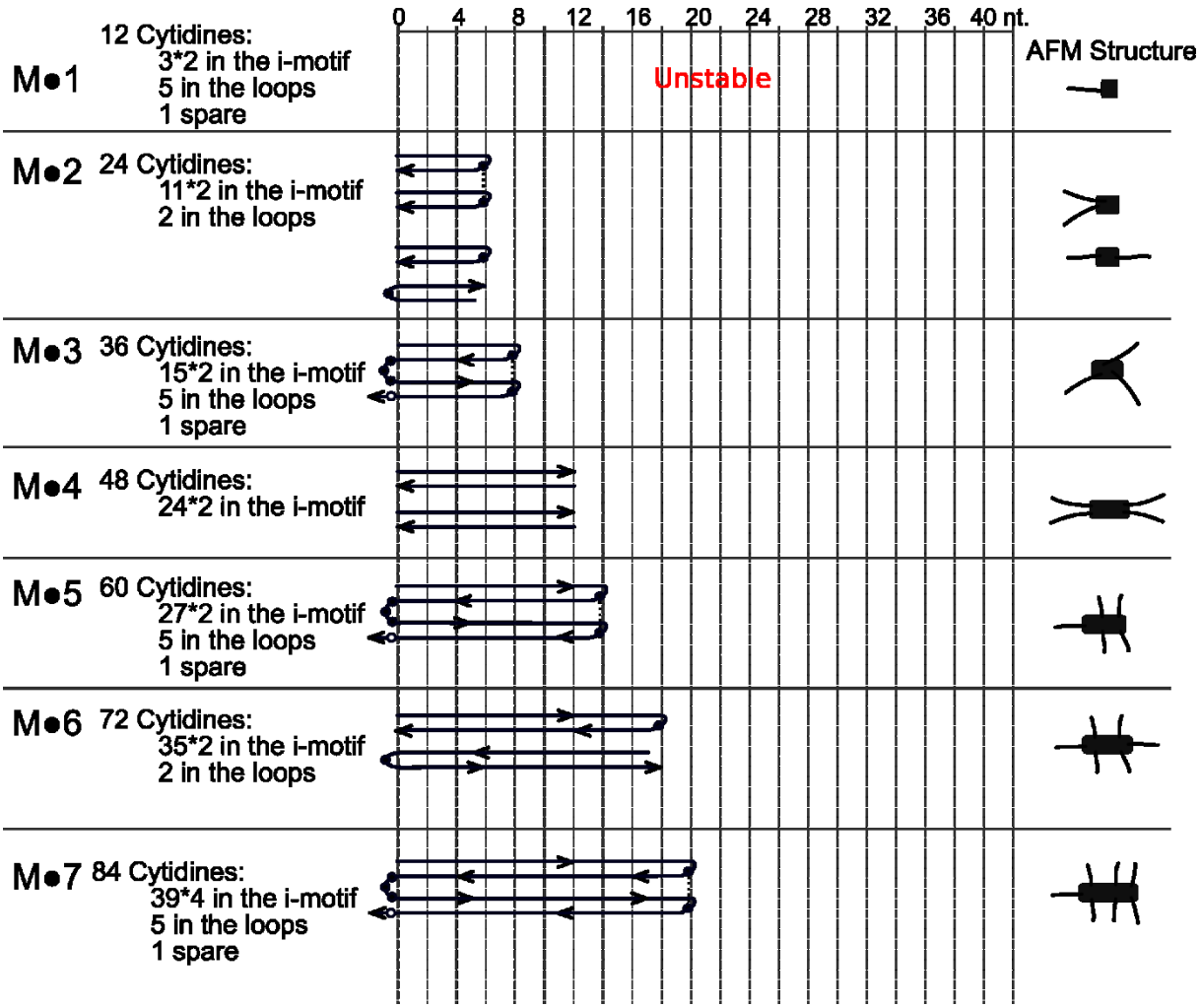

Figure S11. Folding schemes for $C_{12}T_{25}$. Cytidines included in the loops are shown with filled circles, spare cytidines are shown with empty circles. The T_{25} 3'-ends of oligonucleotides are shown with arrows. Potential hydrogen bonds between the oligonucleotides in the minor loops are shown with black dotted lines.

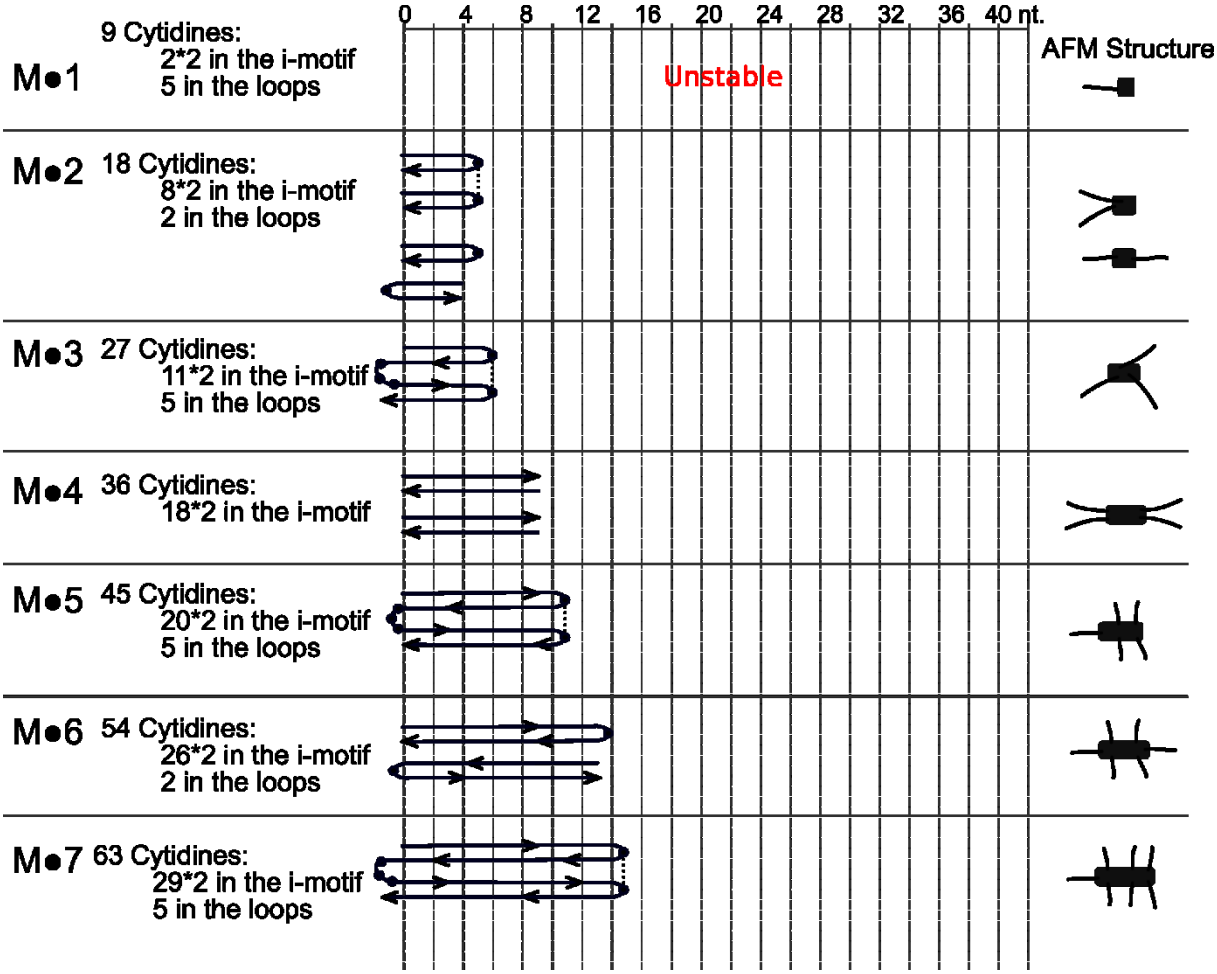

Figure S12. Folding schemes for C_9T_{25}. Cytidines included in the loops are shown with filled circles, spare cytidines are shown with empty circles. The T_{25} 3'-ends of oligonucleotides are shown with arrows. Potential hydrogen bonds between the oligonucleotides in the minor loops are shown with black dotted lines.

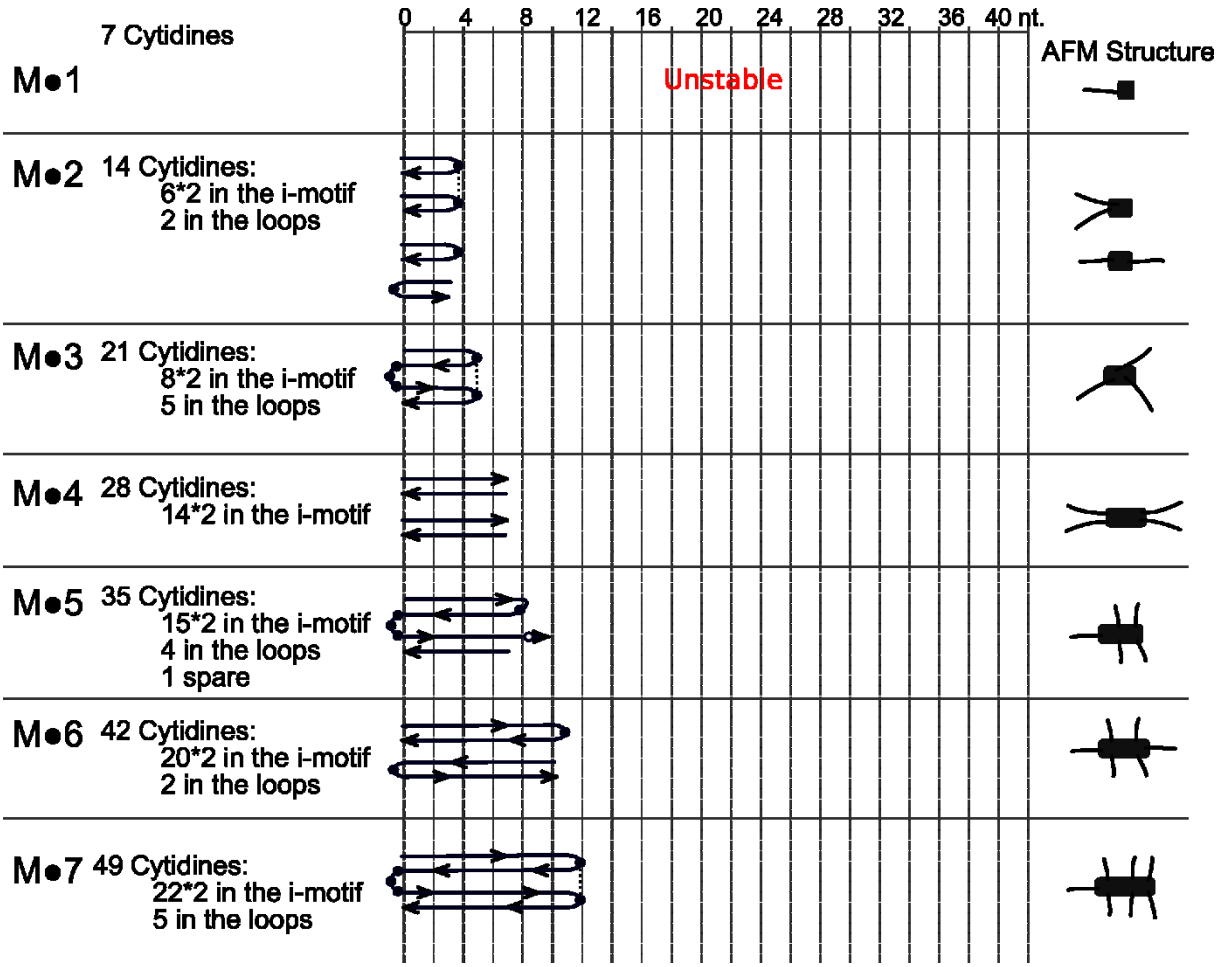

Figure S13. Folding schemes for C_7T_{25}. Cytidines included in the loops are shown with filled circles, spare cytidines are shown with empty circles. The T_{25} 3'-ends of oligonucleotides are shown with arrows. Potential hydrogen bonds between the oligonucleotides in the minor loops are shown with black dotted lines.

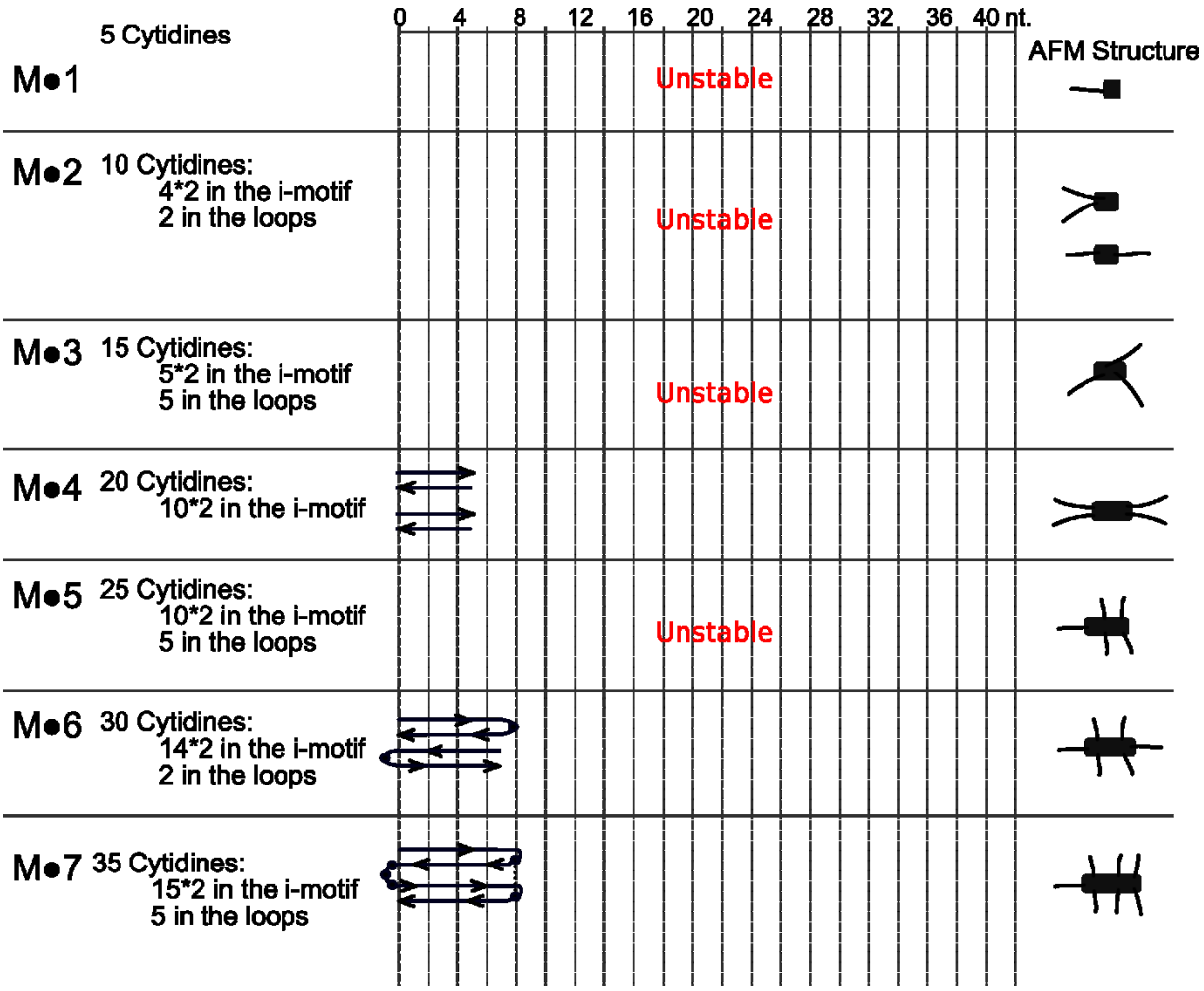

Figure S14. Folding schemes for C_5T_{25}. Cytidines included in the loops are shown with filled circles, spare cytidines are shown with empty circles. The T_{25} 3'-ends of oligonucleotides are shown with arrows. Potential hydrogen bonds between the oligonucleotides in the minor loops are shown with black dotted lines.